THE JOURNAL OF PHYSICAL CHEMISTRY B

Article

pubs.acs.org/JPCB

Tautomerization in the UDP-Galactopyranose Mutase Mechanism: A DFT-Cluster and QM/MM Investigation

WenJuan Huang and James W. Gauld*

Department of Chemistry and Biochemistry, University of Windsor, Windsor, Ontario N9B 3P4, Canada

Supporting Information

ABSTRACT: UDP-galactopyranose mutase (UGM) is a key flavoenzyme involved in cell wall biosynthesis of a variety of pathogenic bacteria and hence, integral to their survival. It catalyzes the interconversion of UDP-galactopyranose (UDP-Gal*p*) and UDP-galactofuranose (UDP-Gal*f*); interconversion of the galactose moieties six- and five-membered ring forms. We have synergistically applied both density functional theory (DFT)-cluster and ONIOM quantum mechanics/molecular mechanics (QM/MM) hybrid calculations to elucidate the mechanism of this important enzyme and to provide insight into its uncommon mechanism. It is shown that the flavin must initially be in its fully reduced form. Furthermore, it requires an $N5_{FAD}$−H proton, which, through a series of tautomerizations, is transferred onto the ring oxygen of the substrate's Gal*p* moiety to facilitate ring-opening with concomitant Schiff base formation. Conversely, Gal*f* formation is achieved via a series of tautomerizations involving proton transfer from the galactose's $-O4_{Gal}H$ group ultimately onto the flavin's $N5_{FAD}$ center. With the DFT-cluster model, the overall rate-limiting step with a barrier of 120.0 kJ mol^{-1} is the interconversion of two Gal*f*-flavin tautomers: one containing a $C4_{FAD}$−OH group and the other a tetrahedral protonated-$N5_{FAD}$ center. In contrast, in the QM/MM model a considerably more extensive chemical model was used that included all of the residues surrounding the active site, and modeled both their steric and electrostatic effects. In this approach, the overall rate-limiting step with a barrier of 99.2 kJ mol^{-1} occurs during conformational rearrangement of the Schiff base linear galactose−flavin complex. This appears due to the lack of suitable functional groups to facilitate the rearrangement.

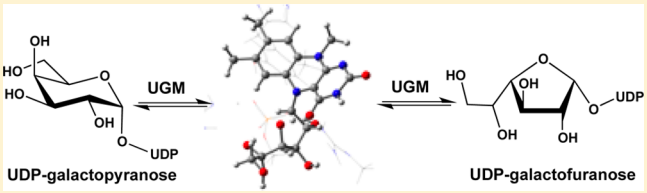

1. INTRODUCTION

Tuberculosis (TB), the well-known disease caused by the pathogenic bacterium *Mycobacteria tuberculosis*, has long afflicted humans. It has been estimated that in 2011 it infected 8.8 million people and resulted in 1.1 million deaths.[1] Unfortunately, the increasing prevalence of multidrug-resistant TB presents major challenges to its diagnosis and present treatments.[1−3] Galactofuranose (Gal*f*) is a key component of a complex peptidoglycan essential for the cell walls of *M. tuberculosis*.[4,5] Its precursor, UDP-galactofuranose (UDP-Gal*f*), is synthesized by the flavoenzyme UDP-galactopyranose mutase (UGM), which catalyzes its formation from UDP-galactopyranose (UDP-Gal*p*) via the overall reaction shown in Scheme 1.[6] Importantly, UGM has been shown to be essential for the growth and survival of *M. tuberculosis*[1,7] and many other pathogenic bacteria such as *Escherichia coli*[8] and *Klebsiella pneumoniae*.[9−11] Furthermore, Gal*f* does not occur in human cells.[5,12] Therefore, UGM represents a logical target for new TB therapeutic drugs[1,13] that are potentially more effective and less toxic to human cells.[5,7,14−21]

Scheme 1. The Overall Mutase Reaction Catalyzed by UGM

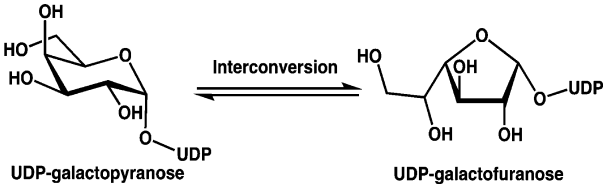

A number of experimental investigations on UGM have appeared in the literature including X-ray crystallographic, spectroscopic, and kinetic analyses, and mutagenesis studies.[6,9,17,18,21−26] However, a clear understanding of its catalytic mechanism has proven elusive due in part to the fact that UGM binds both NADP(H) and the highly redox-sensitive cofactor FAD.[8] The latter provides further complications due to its complex redox and protonation states as a result of its isoalloxazine ring that make it unique among coenzymes.[27,28] For example, in 1996 Nassau et al. appeared to show a requirement for NAD(P)H in order to synthesize UDP-Gal*f*; meanwhile they noted that UGM is a flavoenzyme.[8,11,29] Liu and co-workers later suggested that it instead uses an oxidized FAD to abstract a hydride from the substrate.[21,30] Furthermore, they also proposed that the mechanism involves an oxygen-bridged cage-like galactose intermediate.[21,30] In contrast, Sanders et al.[9] alternatively concluded that the flavin cofactor is in fact fully reduced and suggested that it may act to transfer

Received: November 6, 2012
Revised: November 11, 2012
Published: November 13, 2012

dx.doi.org/10.1021/jp310952c | J. Phys. Chem. B 2012, 116, 14040−14050

Scheme 2. The Catalytic Mechanism of UGM as Proposed by Soltero-Higgin et al.[10] and Gruber et al.[6] Involving the Formation of a Covalent Bond between the $N5_{FAD}$ Center of FAD and the Anomeric Carbon ($C1_{Gal}$) of UDP-Gal*p*

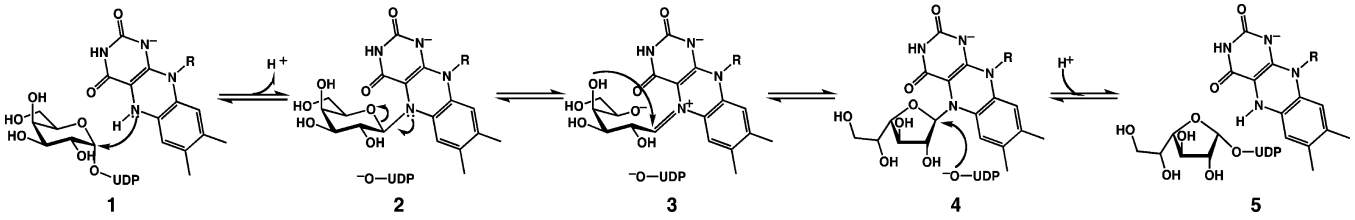

one or two electrons to and from the substrate's sugar during the course of the reaction. Based in part on thermodynamic analyses, however, it has also been put forth that UGM employs a neutral semiquinone radical ($FADH^{\bullet}$)-assisted mechanism.[31,32]

Most recently, Soltero-Higgin et al.[10] concluded that UGM utilizes the fully reduced anionic FAD cofactor, i.e., $FADH^{-}$. Furthermore, they proposed that its catalytic mechanism proceeds via a covalently bonded cofactor-substrate intermediate. More specifically, as shown in Scheme 2,[6] the reduced cofactor's N5 center ($N5_{FAD}$) nucleophilically attacks the anomeric carbon of the substrate sugar ($C1_{Gal}$) via an S_N1 or S_N2 mechanism,[10,16] to give the novel $N5_{FAD}-C1_{Gal}$ covalently bonded intermediate **2**. This reaction occurs with the cleavage of the glycosidic $C1_{Gal}-O-UDP$ bond,[10,16] and it has been suggested that this "could be" the rate-limiting step.[18] Subsequently, opening of the pyranose sugar ring occurs with heterolytic cleavage of the $C1_{Gal}-O5_{Gal}$ bond while the $C1_{Gal}-N5_{FAD}$ link formally changes from a single to a double bond, i.e., formation of the iminium intermediate **3**. A furanose ring intermediate **4** is then formed by nucleophilic attack of the sugars $-O4_{Gal}H$ oxygen at the $C1_{Gal}$ position. A phosphate oxygen of the UDP moiety (O_{UDP}) then attacks at the $C1_{Gal}$ center to give the desired UDP-Gal*f* product and regenerate the reduced $FADH^{-}$ cofactor (Scheme 2).

Additional experimental evidence supporting this proposed mechanism has been obtained. In particular, kinetic isotope studies[24] have also suggested that the $C1_{Gal}-O_{UDP}$ bond is indeed cleaved during the mechanism. Furthermore, saturation transfer difference NMR has been used to examine the binding of the FAD cofactor and the effects of its redox state on its binding.[16,17] They concluded that, compared to the oxidized state, the reduced state has the higher binding affinity to the enzyme–product complex UGM···Gal*f*-UDP. Recently, X-ray crystal structures of the enzyme–substrate complex from different species, including *Klebsiella pneumoniae*,[6,16] *Deinococcus radiodurans*,[14,25] and *Aspergillus fumigatus*,[22,23] have been obtained. These studies provided invaluable insights in the overall enzyme structure, flavin and substrate binding, and enzyme–substrate interactions. Notably, structures were obtained of the UGM···Gal*p*-UDP complex with either reduced or oxidized FAD also bound.[6] Importantly, it was observed that the UDP-Gal*p* and FAD moieties are positioned toward each other when the latter is in its reduced state.[6] In particular, the $C1_{Gal}\cdots N5_{FAD}$ distance is 8.0 Å (PDB ID: 3INR) when the flavin is in an oxidized state but only 3.6 Å (PDB ID: 3INT) when the flavin is reduced. In addition, using the weak reducing agent $NaCNBH_3$, the covalently bonded flavin-imine-intermediate complex was reduced.[6,10]

Several computational investigations on UGM have also appeared in the literature.[17,18,33] These have focused on the application of docking and molecular dynamics (MD) methods to provide insights into the bound substrate and enzyme···substrate interactions. More specifically, the docking studies[33] considered possible bound conformations of the substrate. Later, MD studies[17,18] examined substrate binding and showed that a mobile peptide loop containing an arginyl residue (Arg174) closes over the bound active site. As a result, Arg174 is then able to interact with the substrate's phosphate attached to the sugar ring. One of these also considered binding of the product analogue UDP-[3,F]Gal*f* and its hydrogen bonding interactions with a flavin cofactor and active site residues. Importantly, however, none of these previous investigations examined the catalytic mechanism of UGM.

In this study, density functional theory (DFT) and quantum mechanics/molecular mechanics (QM/MM) methods have been complementarily used, in combination with large active site models, to investigate the mechanism by which UGM catalyzes the conversion of UDP-Gal*p* to UDP-Gal*f*. In particular, the feasibility of the nucleophilic attack of the flavin on the substrate sugar as proposed by Soltero-Higgin et al.[6,10] has been examined. In addition, however, the possible role and importance of both flavin and substrate protons in the overall mechanism both with regards to ring-opening and the mutase itself, and the possible role and consequences of tautomerization, have been considered. These studies not only provide new atomistic-level details into the possible mechanism of UGM, but also provide insights into the physiologically important flavoenzymes in general and, in particular, those that involve substrate–flavin reactions.

2. COMPUTATIONAL METHODS

The Gaussian 09 suite of programs was used for all calculations.[34] The DFT-large active site cluster model calculations utilized the hybrid exchange-correlation functional B3LYP.[35−37] Optimized structures and their harmonic vibrational frequencies were obtained with the 6-31G(d) basis set. Relative energies, with solvation effects included, were then obtained by performing single-point calculations on the above geometries at the B3LYP/6-311+G(2df,p) level within an Integral Equation Formalism Polarizable Continuum Model (IEF-PCM). As is common when including the general polarity of the protein environment around an enzyme active site, a dielectric constant (ε) of 4.0 was used.[38,39] That is, relative energies were obtained at the IEF-PCM(ε = 4.0)-B3LYP/6-311+G(2df,p)//B3LYP/6-31G(d) level of theory. All transition structures (TSs) obtained using this DFT-cluster approach were characterized via calculation of their harmonic vibrational frequencies.

For these DFT-based studies, a large active site cluster model was obtained from an X-ray crystal structure of the enzyme-bound substrate complex (UGM···UDP-Gal*p*) from *K. pneumoniae* (PDB ID: 3INT).[6] It is noted that Partha et al. have obtained the structure of UGM···UDP-Gal*p* from *D. radio-*

dx.doi.org/10.1021/jp310952c | J. Phys. Chem. B 2012, 116, 14040−14050

durans (PDB ID: 3HDQ).[25] Importantly, however, the overall binding mode of the substrate in the two active sites is quite consistent. Indeed, the largest difference in key relevant distances between these two structures was measured to be ~0.5 Å, with the average difference being ~0.3 Å (Table S3). The resulting model based on the crystal structure of UGM···substrate from *K. pneumoniae* is shown in Figure 1. Specifically, the substrate was modeled by 1-methylphosphate-α-Gal*p* while the reduced flavin was represented by lumiflavin.

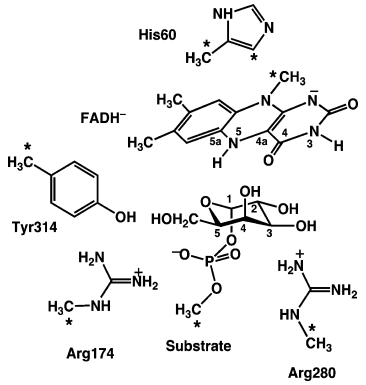

Figure 1. The large fully bound active site model used in the DFT-cluster calculations. Atoms marked by an asterisk (*) were fixed at their X-ray crystal structure (PDB ID: 3INT) position.

In addition, the *R*-groups of the key active site residues Arg174 and Arg280, Tyr314, and His60 were included and modeled by methylguanidinium, 4-methylphenol, and 4-methyl-3H-imidazole, respectively. To ensure the structural integrity of the model, atoms marked by an asterisk in Figure 1 were held fixed at their X-ray crystal structure position. In aqueous solution, histidine's imidazole group has a pK_a of approximately 6.0,[40] but this value can differ within a protein environment. Hence, we considered His60 as neutral or protonated (Figure S1, Supporting Information), which are identified by the superscripts **a** and **b** in corresponding potential energy surfaces (PESs) and for each stationary point. For the latter, the resulting mechanism obtained is less favorable than with a neutral His60 (TS 148.1 kJ mol^{-1}). Thus, for simplicity, hereafter only the mechanism obtained for when His60 is neutral is discussed in detail, unless otherwise noted. The DFT-cluster approach has been successfully applied to study enzymatic mechanisms and reviewed in detail.[41−45]

QM/MM calculations were performed using the two-layer ONIOM method as available in Gaussian 09.[46] Optimized structures and their harmonic vibrational frequencies were obtained at the ONIOM(B3LYP/6-31G(d):Amber)-ME level of theory.[46,47] More accurate relative energies were obtained by performing single point energy calculations on the above optimized structures at the ONIOM(B3LYP/6-311+G(2df,p):AMBER) level of theory within the electronic embedding (EE) formalism.[46] All TSs obtained using this QM/MM approach were also characterized via calculation of their harmonic vibrational frequencies except for TS1, TS5, and TS6, which were instead obtained via detailed systematic scans of the PES.

The QM/MM substrate-bound active site model was also obtained from the above X-ray crystal structure (PDB ID: 3INT), and is shown in Figure 2. Specifically, the QM region included the substrate, Arg174, and Arg280 and the flavin cofactor modeled by 1-methylpyrophosphate-α-Gal*p*, methyl-guanidinium, and lumiflavin, respectively. The MM layer included a number of residues modeled either in their entirety or only including their backbone or R-group (see Figure 2). In

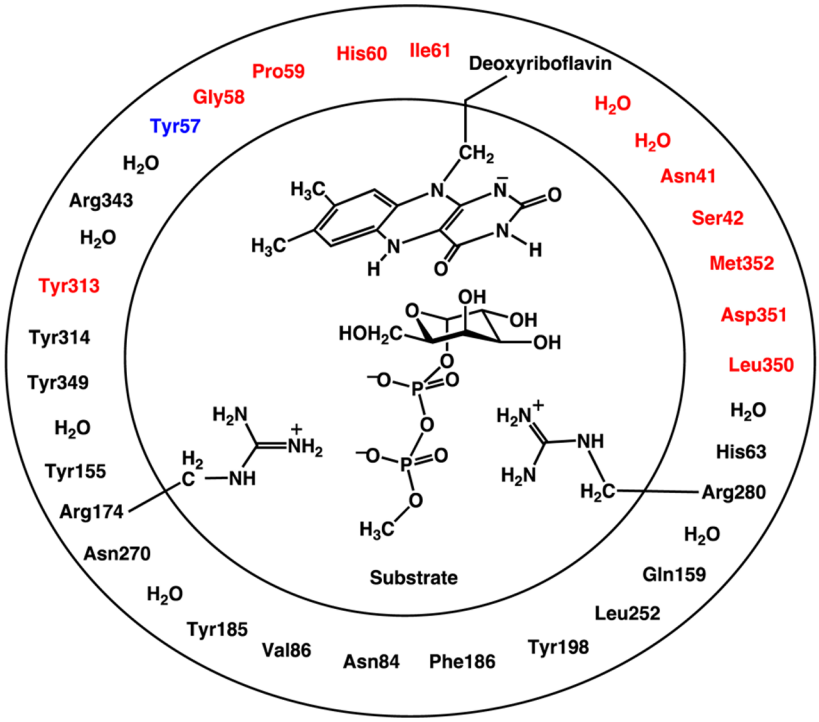

Figure 2. The QM/MM substrate-bound active site model: the inner circle indicates those moieties placed in the QM layer, while the outer circle indicates those placed in the MM layer. Residue color code: included in their entirety (red); backbone was included with the *R*-group modeled by a methyl (blue); only *R*-groups included (black).

dx.doi.org/10.1021/jp310952c | *J. Phys. Chem. B* 2012, 116, 14040−14050

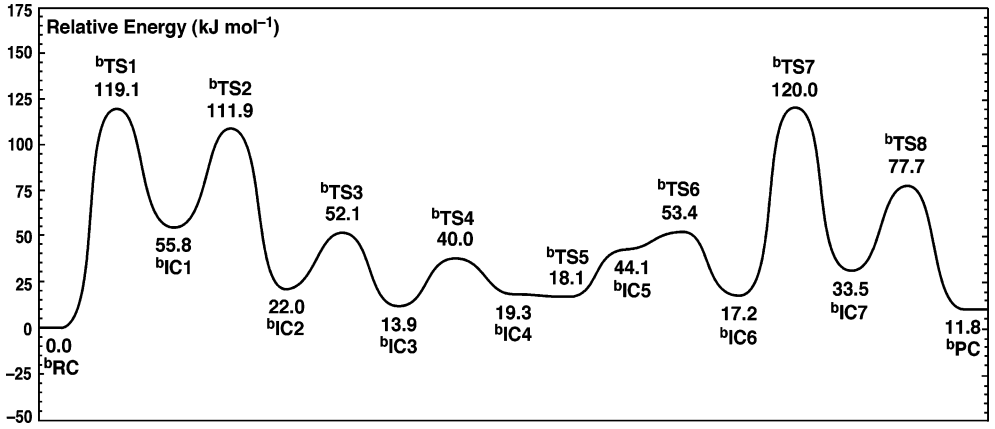

Figure 3. PES for the catalytic mechanism of UGM (with a neutral His60) obtained at the IEFPCM(ε = 4.0) B3LYP/6-311+G(2df,p)//B3LYP/6-31G(d) level of theory.

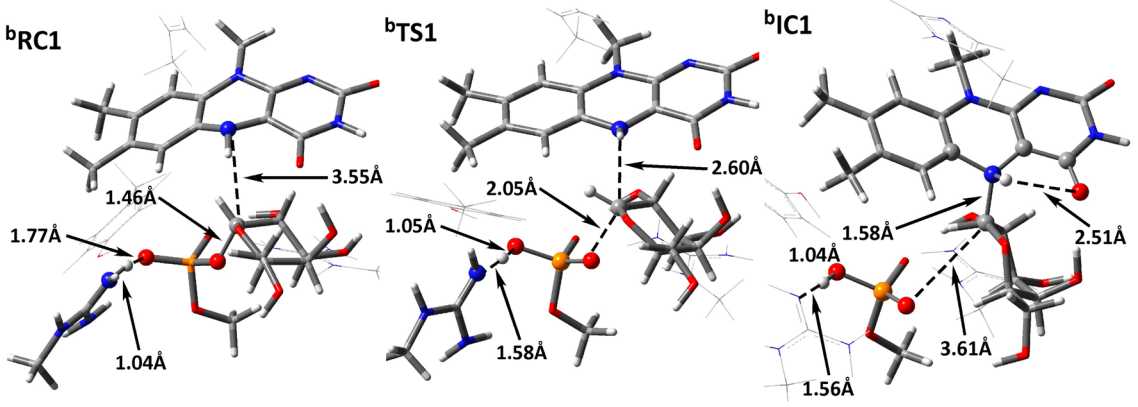

Figure 4. Optimized structures with selected bond lengths (angstroms) of ^{b}RC, ^{b}TS1 and ^{b}IC1 (see text). For clarity, only some residues are shown in ball and stick format. Color key: C (gray); O (red); N (blue); P (orange); H (white).

addition, several H_2O observed in the X-ray crystal structure were included in the MM layer. Certain atoms in each residue were held fixed at their X-ray crystal structure position so as to maintain the integrity of the model (Table S2).

3. RESULTS AND DISCUSSION

3.1. Deprotonation of the Initial Flavin Cofactor. As detailed in the Introduction, the mechanism proposed by Soltero-Higgin and co-workers[6,10] involves the attack of the fully reduced anionic $FADH^-$ cofactor on the anomeric center. Unfortunately, while the attack is known to occur, the means by which the proton from the $N5_{FAD}$−H group is lost remains unclear (i.e., formation of **2** in Scheme 2). In the X-ray crystal structure of UGM with bound flavin cofactor and substrate (PDB ID: 3INT), His60 is the only polar-basic residue that may be within hydrogen bonding distance of $N5_{FAD}$−H; $r(N5_{FAD}\cdots NHis_{60})$ = 3.70 Å, and thus able to act as a base. Experimentally, the aqueous solution pK_a of the R-group imidazole of histidine has been measured to be ∼6. Meanwhile, that of N5−H in $FADH^-$ has been determined using NMR to be considerably higher at ≥20.[42,50] In fact, the authors noted that the value placed "specific constraints" on the ability of reduced flavin to participate in reactions via deprotonation of its N5−H moiety. It is noted that the latter value has been previously calculated within a protein environment using QM/MM to be 14, which is still markedly higher than that of His or water.[51] Indeed, in this present study the proton affinity of the imidazole of His60 (1161.9 kJ mol^{-1}) is calculated to be markedly less than that of FAD^{2-} (1521.1 kJ mol^{-1}) within a protein-like environment.[48] Thus, His60 is unlikely to be able to deprotonate the $FADH^-$ cofactor.

Another possibility is that a phosphate of the UDP moiety resulting from the proposed transient dissociation of the substrate may act as the base. However, within the above same X-ray crystal structure (PDB ID: 3INT), the shortest distance between a UDP phosphate oxygen (O_{UDP}) and $N5_{FAD}$ is approximately 5 Å. Furthermore, these two groups are positioned on almost opposite sides of the substrate's galactose ring. Hence, the UDP moiety is also unlikely to be able to deprotonate $N5_{FAD}$−H. Also, no water is observed in the UGM active site in the above crystal structure within a distance of 4 Å of the $N5_{FAD}$ center, and the isoalloxazine ring of the cofactor is sequestered from the surrounding solvent.[6] Consequently, and given the high pK_a of $N5_{FADH-}$, it would seem unlikely that the $N5_{FAD}$−H proton is lost to an active site water or the aqueous solvent.

3.2. Catalytic Mechanism Obtained Using the DFT-Cluster Model. Alternatively, however, the nitrogen of the $FADH^-$ cofactor's $N5_{FAD}$−H group may directly nucleophilically attack the substrate's anomeric C1 carbon, that is, without deprotonation of the $N5_{FAD}$−H group. The PES obtained for the resulting mechanism is shown in Figure 3.

3.2.1. Formation of a Flavin-Substrate ($N5_{FAD}$—$C1_{Gal}$) Covalent Bond. In the fully bound active site (^{b}RC), the $N5_{FAD}$

dx.doi.org/10.1021/jp310952c | J. Phys. Chem. B 2012, 116, 14040−14050

center of the cofactor is positioned 3.55 Å from the substrate's $C1_{Gal}$ center, almost opposite the substrate's phosphate group (Figure 4). In addition, it is slightly pyramidal as indicated by a ∠H5−N5−C4a−C4 dihedral angle of −15.0° (see Figures 1 and S2 for $FADH^-$ numbering).

The first step of the UGM mechanism is the formation of a covalent bond between the $FADH^-$ isoalloxazine ring and the substrate's Gal*p* ring. More specifically, the Gal*p* ring is located beneath the *re* face of the isoalloxazine ring of $FADH^-$, while the imidazole of His60 sits atop its *si* face.[22] As a result, the cofactor's $N5_{FAD}$ center must invert and nucleophilically attacks the anomeric carbon ($C1_{Gal}$) from above the Gal*p* ring while the $C1_{Gal}$—O_{UDP} bond is concomitantly cleaved. This S_N2-type reaction step proceeds via the transition structure ^{b}TS1 with a barrier of 119.1 kJ mol^{-1} relative to the reactant complex ^{b}RC. Thus, given the nature of ^{b}TS1, the rate of attack would be affected with any change in the nucleophilicity of the cofactor's $N5_{FAD}$. Such an effect would not be seen for an S_N1-type reaction. The resulting tetrahedral-$N5_{FAD}$ FAD-substrate covalent intermediate ^{b}IC1 is higher in energy than ^{b}RC by only 55.8 kJ mol^{-1}. It is noted that the charge on the isoalloxazine ring, calculated using natural bond orbital (NBO) analyses, has gone from −0.89 (^{b}RC) to 0.35.

In ^{b}IC1, an elongated $N5_{FAD}$—C_{Gal} single-bond of length 1.58 Å has now been formed. In addition, the ∠$H5_{FAD}$−$N5_{FAD}$−$C4a_{FAD}$−$C4_{FAD}$ dihedral angle has increased to 42.9°, indicating that $N5_{FAD}$ has increased sp^3 character. Meanwhile, the cleaved methyl-phosphate group has been stabilized and neutralized by accepting a proton from Arg280. However, it continues to interact with Arg280 via a quite short and strong hydrogen bond (1.56 Å), slightly shorter than that observed in ^{b}RC (1.77 Å; Figure 4). It should also be noted that the $N5_{FAD}$—H bond has lengthened marginally from that observed in ^{b}RC (1.02 Å) to 1.03 Å (Table S2).

It is noted that for the corresponding fully bound active site model in which His60 is protonated, the $N5_{FAD}\cdots C1_{Gal}$ distance in the initial reactant complex (^{a}RC; Table S2) is slightly shorter at 3.41 Å. However, the barrier for this first reaction step is significantly higher at 140.9 kJ mol^{-1} (Figure S1). Importantly, this is markedly higher than that obtained for the catalytic process with neutral His60.

3.2.2. Substrate Sugar Ring-Opening via Tautomerization. It has been noted that sugar ring-opening processes are usually initiated by ring oxygen protonation reactions.[40,49,50] In ^{b}IC1, the now tetrahedral $N5_{FAD}$−H could potentially act as the proton donor. However, direct transfer onto the pyranose ring oxygen ($O5_{Gal}$) would necessarily require a strained four-member ring transition structure. These are generally inherently high in energy. Indeed, the barrier for such a reaction process is calculated to be 189.7 kJ mol^{-1} with respect to ^{b}RC (Table S2). These are significantly higher than the upper activation energy limit of enzymes[45,51] and thus, unlikely to be feasible.

However, in ^{b}IC1, the $N5_{FAD}$−H group forms a weak intramolecular hydrogen bond with the $C4_{FAD}$=O oxygen; $r(N5_{FAD}H\cdots OC4_{FAD})$ = 2.51 Å (Figure 4). In fact, the FAD−sugar moiety can tautomerize by an intramolecular proton transfer from $N5_{FAD}$−H to the $C4_{FAD}$=O carbonyl oxygen. This proceeds via the five-membered ring transition structure ^{b}TS2 (Figure 5) at a cost of only 56.1 kJ mol^{-1} with respect to ^{b}IC1 and 111.9 kJ mol^{-1} with respect to ^{b}RC (Figure 3). This barrier is less than that for the preceding nucleophilic attack of

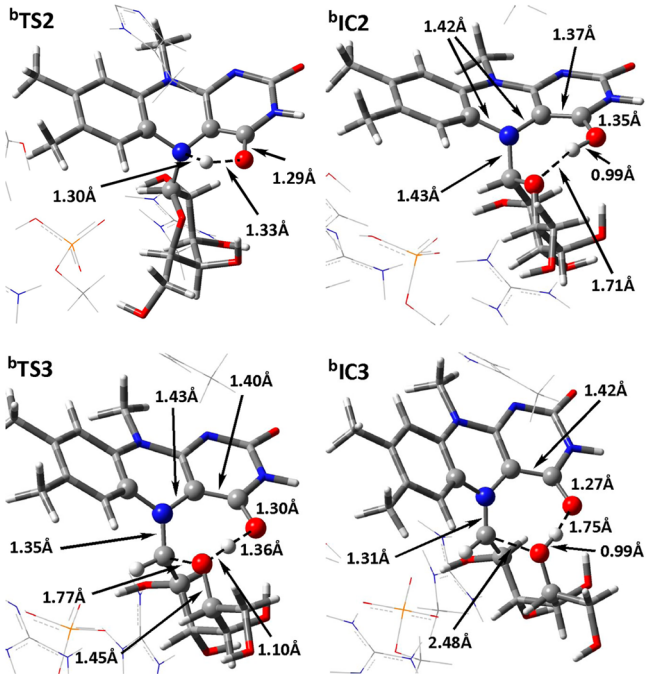

Figure 5. Optimized structures with selected bond lengths (Angstroms) of ^{b}TS2, ^{b}IC2, ^{b}TS3 and ^{b}IC3 (see text). For clarity, only some residues are shown in ball and stick format. Color key: C (gray); O (red); N (blue); P (orange); H (white).

$N5_{FAD}$ at C1 of the substrate. Furthermore, it is also markedly lower than for direct proton transfer from $N5_{FAD}$−H onto the pyranose's $O5_{Gal}$ center via a four-membered ring TS (see above) and in fact is now enzymatically feasible.

The resulting tautomeric intermediate ^{b}IC2 formed lies quite low in energy: 33.8 kJ mol^{-1} lower in energy than ^{b}IC1, or just 22.0 kJ mol^{-1} above that of the initial bound active site ^{b}RC. It is noted that this relative energy trend for the tautomers of the covalent intermediates is the opposite of that observed for the isolated initial $FADH^-$ cofactor (Table S2). In ^{b}IC2, the $N5_{FAD}$−$C1_{Gal}$ bond formed in the first step has shortened significantly by 0.15 Å to 1.43 Å, and is now slightly shorter than a typical C−N single bond (e.g., $r(H_3C{-}NH_2)$ = 1.44 Å).[52] The change in hybridization of the $N5_{FAD}$ center (sp^3 to sp^2) is further highlighted by the decrease in the angle ∠$N5_{FAD}$−$C5a_{FAD}$−$C4a_{FAD}$−$C1_{Gal}$ from 27.6° (^{b}IC1) to 13.2° (^{b}IC2). Related shortenings in the $N5_{FAD}$—$C4a_{FAD}$ and $N5_{FAD}$—$C5a_{FAD}$ bonds are also observed from 1.47 and 1.48 Å, respectively, to 1.42 Å each, while the $C4_{FAD}$—$O4_{FAD}$ bond has lengthened to 1.35 Å (Figure 5).

Notably, in ^{b}IC2, the newly formed −$O4_{FAD}$H group forms a short strong hydrogen bond (1.71 Å) with the sugar ring's $O5_{Gal}$ center. Thus, the proton is now well-placed to transfer onto the substrate's sugar ring oxygen. An alternative is that a neighboring hydroxyl group on the sugar ring may facilitate ring-opening. Of the hydroxyl groups on the ring, only $C4_{Ga}$−OH is in the vicinity of $O5_{Gal}$. Thus, if a protein residue near that OH group could participate in a H-bonding relay, such a process might be possible. Regrettably, such a residue does not exist. Rather $C4_{Ga}$−OH sits in a hydrophobic pocket. Thus, it appears that the only group suited to participate in transfer onto the substrate's sugar ring oxygen is the newly formed −$O4_{FAD}$H group. Indeed, such a process proceeds via the seven-membered ring transition structure ^{b}TS3 with a barrier of

dx.doi.org/10.1021/jp310952c | J. Phys. Chem. B 2012, 116, 14040−14050

only 30.1 kJ mol^{-1} relative to ^{b}IC2 and 52.1 kJ mol^{-1} with respect to ^{b}RC. It is noted that in ^{b}TS3 the $C1_{Gal}$—$O5_{Gal}$ bond has lengthened significantly by 0.31 Å to 1.77 Å. Concomitantly, the $-O4_{FAD}H$ proton is essentially wholly transferred onto $O5_{Gal}$ as illustrated by the fact that $r(O5_{Gal}\cdots H)$ = 1.10 Å (Figure 5), thus helping to stabilize the charge build-up on $O5_{Gal}$. Notably, the $N5_{FAD}$–$C1_{Gal}$ bond has shortened by 0.12–1.35 Å, indicating a marked increase in double-bond character. Additional changes are also observed in the cofactor's structure such as shortening of the C4—O bond and lengthening of both the C4a—C4 and N5—C4a bonds (Figure 5). This also seems to suggest that proton transfer from the cofactor tautomer onto $O5_{Gal}$ and the resulting associated changes within the cofactor may in fact help facilitate ring-opening of the sugar.

It is noted that the resulting Z-conformer imine is not expected by steric predictions (i.e., the E-conformer would result in less steric clash between the cleaved sugar ring and the flavin moiety). However, the resulting imine covalent linear sugar–flavin tautomer ^{b}IC3 lies 8.1 kJ mol^{-1} lower in energy than the preceding glycosidic bonded cyclic sugar–flavin tautomer ^{b}IC2. That is, it now lies just 13.9 kJ mol^{-1} higher in energy than ^{b}RC (Figure 4). Furthermore, the formation of the Z-conformer prevents any steric clash that would occur between the cleaved UDP moiety and sugar ring. In ^{b}IC3, the $C1_{Gal}\cdots O5_{Gal}$ distance has increased markedly to 2.48 Å, that is, the bond has broken and the galactose is now in a linear conformation (Figure 5). In addition, the $N5_{FAD}$=$C1_{Gal}$ distance has decreased even further to just 1.31 Å. The newly formed $-O5_{Gal}H$ group, however, remains hydrogen bonded to the cofactor's $C4_{FAD}$=O oxygen. It is noted that sugar ring-opening with formation of a neutral $-O5_{Gal}H$ group rather than the proposed anionic $-O5_{Gal}^{-}$ moiety[6,10] may enable nucleophilic attack of the $-O4_{Gal}H$ oxygen at the $C1_{Gal}$ center to be competitive with reattack by $O5_{Gal}$. In addition, because $C1_{Gal}$–O5 bond cleavage occurs with concomitant formation of the $C1_{Gal}$=$N5_{FAD}$ double bond, only the stereoisomer of ^{b}IC3 shown in Figure 6 is obtained. It is noted that the resulting Z-conformer imine is not expected by steric predictions (i.e., the E-conformer would result in less steric clash between cleaved sugar ring and flavin moiety).

The above observed reaction steps also provide insights into the experimental[6,9] observation that the catalytic mechanism of UGM requires a fully reduced flavin cofactor: the oxidized form rendering the enzyme inactive.[6,23,25,26] In particular, the reduced form is required in order to be able to nucleophilically attack the C1 center of the galactose sugar ring, and eventually form the $N5_{FAD}$=$C1_{Gal}$ double bond. Furthermore, the $N5_{FAD}$–H proton, lacking in oxidized FAD, is required for the ring-opening process and neutralization of the $O5_{Gal}$ center.

3.2.3. Conformational Rearrangement of the Linear Sugar Moiety. In ^{b}IC3 the $-O4_{Gal}H$ group is also hydrogen bonded with the $C4a_{FAD}$=O moiety, $r(O4_{Gal}H\cdots OC4)$ = 1.80 Å. More importantly, however, it is not suitably positioned for nucleophilic attack at $C1_{Gal}$ to form the desired Galf ring. Hence, the linear sugar moiety must first undergo an appropriate conformational rearrangement. Such a process can be achieved via two sequential rotations.

First, the $-O5_{Gal}H$ group rotates such that rather than being hydrogen bonded to the $C4_{FAD}$=O oxygen, it instead forms a hydrogen bond with a phosphate oxygen of the initial substrate's cleaved but still active site-bound UDP moiety. More specifically, this conformational change occurs via ^{b}TS4 with a barrier of only 26.1 kJ mol^{-1} relative to ^{b}IC3 to give ^{b}IC4

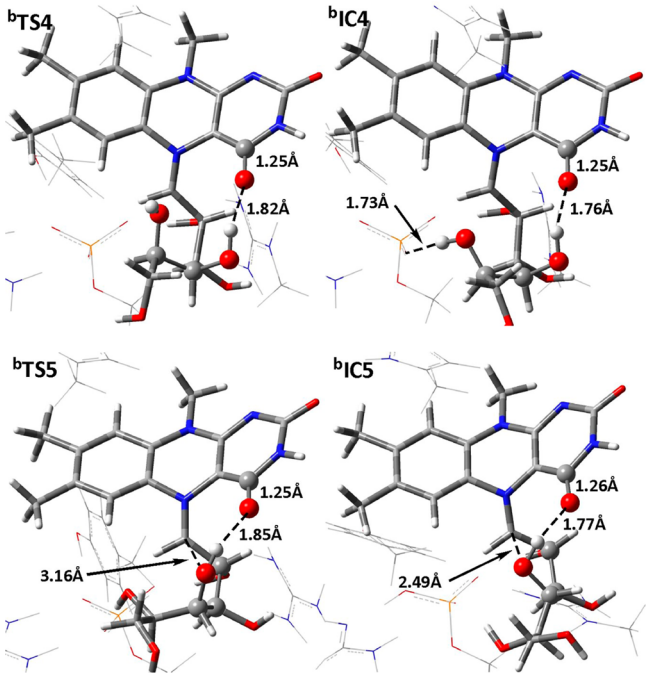

Figure 6. Optimized structures with selected bond lengths (angstroms) of ^{b}TS4, ^{b}IC4, ^{b}TS5, and ^{b}IC5 (see text). For clarity, only some residues are shown in ball and stick format. Color key: C (gray); O (red); N (blue); P (orange); H (white).

lying just 5.4 kJ mol^{-1} higher in energy than ^{b}IC3. Importantly, structurally in ^{b}IC4 the $\angle O4_{FAD}$–$C5_{Gal}$–$O5_{Gal}$–$H5_{Gal}$ dihedral angle has changed from −13.2° (^{b}IC3) to 137.0°. This indicates that the $-O5_{Gal}H$ group is now directed away from the $C4_{FAD}$=O and toward a UDP phosphate oxygen with which it now forms a short strong hydrogen bond (1.73 Å). It is also noted that this rotation also induces a slight shift in the positioning of the sugar moieties $-O4_{Gal}H$ group. In particular, the $-O4_{Gal}H\cdots OC4_{FAD}$ hydrogen bond has shortened and strengthened slightly by 0.04 Å to 1.76 Å (Figure 6).

However, as can be seen in Figure 6, the $O4_{Gal}$ oxygen in ^{b}IC4 is still not ideally positioned to nucleophilically attack the $C1_{Gal}$ center, necessary for formation of the Gal*f* ring. Hence, a further shift in the positioning of the $-O4_{Gal}H$ hydroxyl group is required. More specifically, it undergoes a rotation around the sugar moieties' C3—C4 bond via the transition structure ^{b}TS5 to give the alternative conformer ^{b}IC5 lying just 24.8 kJ mol^{-1} higher in energy than ^{b}IC4 (Figure 3). It is noted that the relative energy of ^{b}TS5 is slightly lower than that of ^{b}IC4. This is a common artifact of single-point energy calculations with corrections (e.g., solvation). It simply indicates that within the present DFT-cluster model, ^{b}IC5 is predicted to be able to rearrange essentially without a barrier back to ^{b}IC4. Structurally, in ^{b}IC5, the $-O4_{Gal}H$ group still maintains a short strong hydrogen bond with the $C4_{FAD}$=O group (1.77 Å). More importantly, however, $O4_{Gal}$ is now orientated over the $C1_{Gal}$ center with an $O4_{Gal}\cdots C1_{Gal}$ distance of only 2.49 Å (Figure 6). Thus, it is now better situated for the nucleophilic attack at $C1_{Gal}$ than $O5_{Gal}$, which has further shifted position slightly but remains hydrogen bonded to a UDP phosphate oxygen.

3.2.4. Formation of the Galf Ring. This third and final stage of the overall catalytic mechanism is in essence the analogous reverse of the initial substrate reaction with the $FADH^{-}$

dx.doi.org/10.1021/jp310952c | J. Phys. Chem. B 2012, 116, 14040–14050

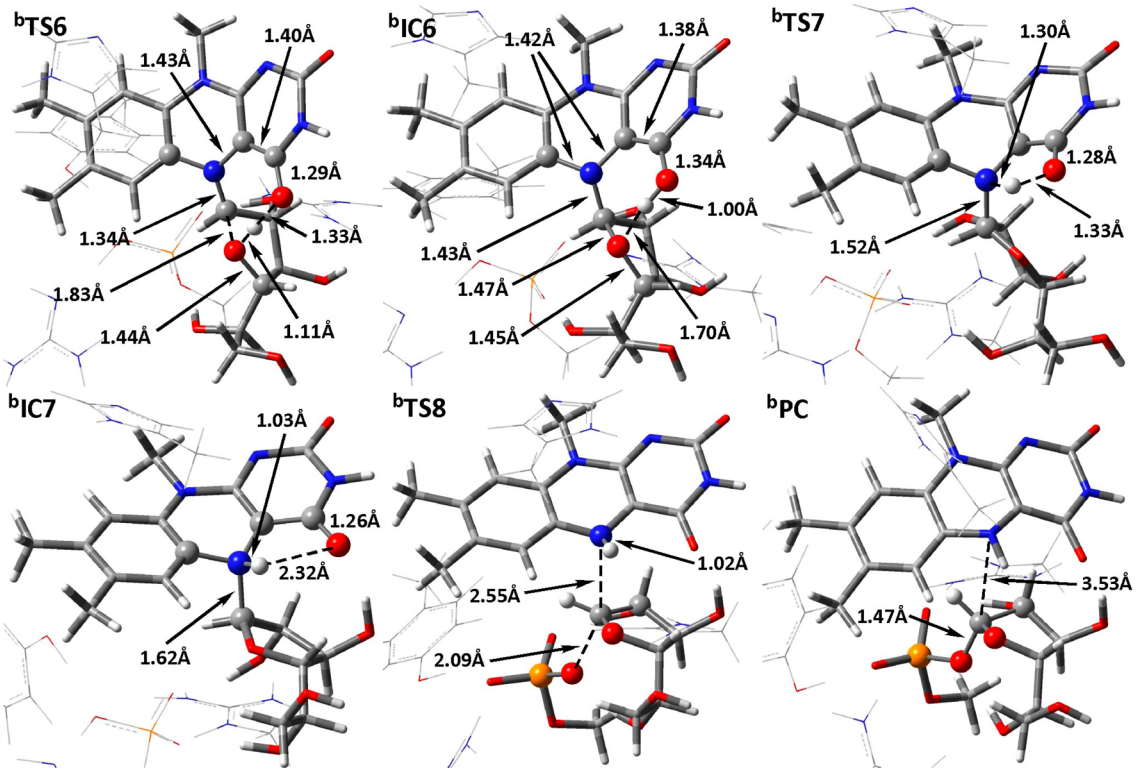

Figure 7. Optimized structures with selected bond lengths (angstroms) of ^{b}TS6, ^{b}IC6, ^{b}TS7, ^{b}IC7, ^{b}TS8, and ^{b}PC (see text). For clarity, only some residues are shown in ball and stick format. Color key: C (gray); O (red); N (blue); P (orange); H (white).

Scheme 3. Schematic Summary of the Reactant, Intermediates, and Product Complexes Obtained for the Overall Mechanism of UGM Using the DFT-Cluster Approach (See Text)

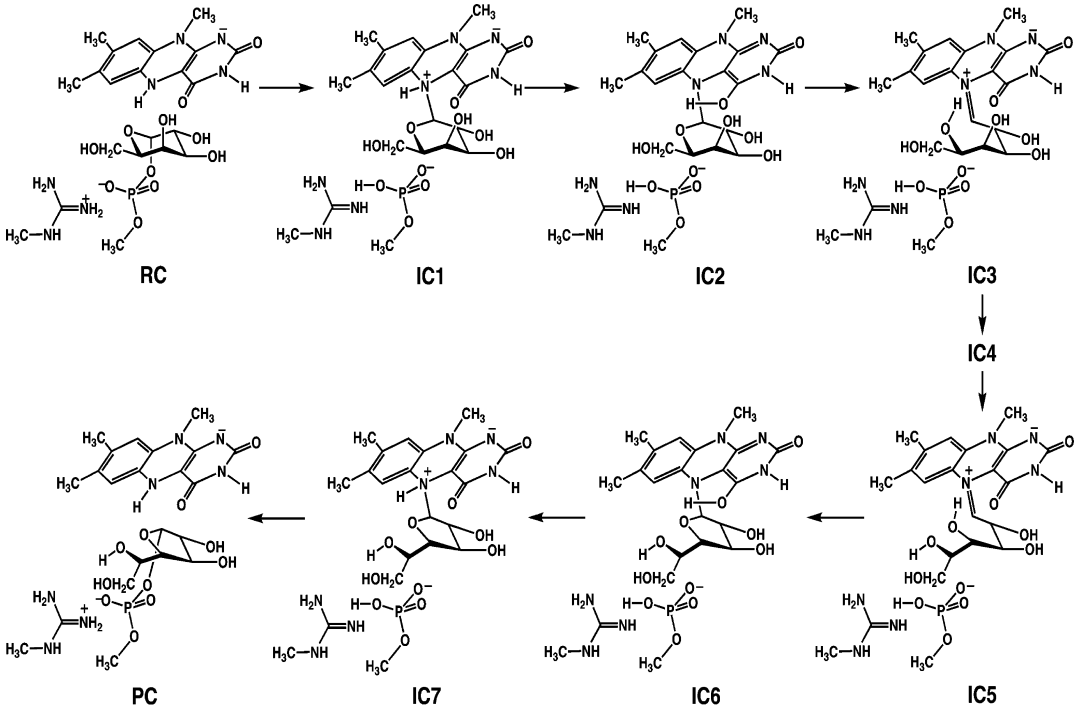

cofactor and the subsequent ring-opening process (see sections 3.2.1 and 3.2.2).

For instance, it is initiated by nucleophilic attack of the $-O4_{Gal}H$ hydroxyl's oxygen at the $C1_{Gal}$ center with concomitant transfer of its proton to the cofactor moieties $C4_{FAD}$=O carbonyl oxygen. This reaction occurs via the seven-membered ring transition structure ^{b}TS6 and requires just 9.3 kJ mol^{-1} with respect to ^{b}IC5 to give the furanose-containing intermediate ^{b}IC6. The latter species lies quite low in relative energy at 17.2 kJ mol^{-1} above that of ^{b}RC (Figure 3). Notably,

dx.doi.org/10.1021/jp310952c | J. Phys. Chem. B 2012, 116, 14040−14050

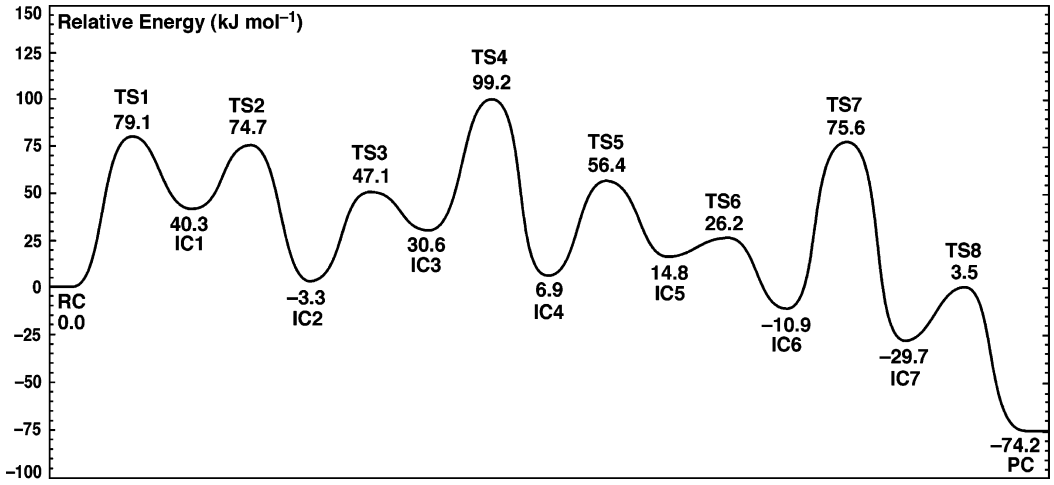

Figure 8. PES for the catalytic mechanism of UGM (with a neutral His60) obtained at the ONIOM(B3LYP/6-311+G(2df,p):AMBER96)-EE//ONIOM(B3LYP/6-31G(d):Amber96)-ME level of theory.

as can be seen in Figure 7, in ^{b}IC6 the cofactor moiety has now regenerated its C4−OH containing tautomer. Furthermore, the protonation of the cofactor's $C4_{FAD}$−O oxygen has caused a significant lengthening in its bond by 0.08 Å to 1.34 Å. This concomitantly induces modest shortenings in both the $C4a_{FAD}$—$C4_{FAD}$ and $N5_{FAD}$—$C4a_{FAD}$ bonds. Consequently, the $C1_{Gal}$–$N5_{FAD}$ cross-link has lengthened significantly to 1.43 Å, such that it now resembles a more typical N-glycosidic single bond. Importantly, the $C1_{Gal}$—$O4_{Gal}$ distance has also decreased markedly by 1.02 Å to just 1.47 Å, a typical C−O single bond length. It is noted that the furanose−flavin tautomer complex ^{b}IC6 is marginally lower in energy by 4.8 kJ mol^{-1} than the analogous pyranose-containing complex ^{b}IC2 (Figure 3).

The subsequent reaction step is formation of the $N5_{FAD}$−H containing tautomer, in which the flavin moiety is now covalently bonded with the furanose, that is, transfer of the proton from the $C4_{FAD}$−OH group onto the spatially adjacent $N5_{FAD}$ center. This occurs via the five-membered ring transition structure ^{b}TS7 at a cost 120.0 kJ mol^{-1} relative to the initial reactant complex ^{b}RC (Figure 3). This is the highest reaction barrier calculated overall for the UGM catalytic mechanism using the present DFT-cluster model, and is close to the generally held upper activation barriers of enzymatic mechanisms.[45,51] This likely reflects in part the computational model (see below), the constrained ring involved in the transfer, and structural changes such as slight deformation of the flavin and breaking of the $O4_{Gal}$···$HOC4_{FAD}$ hydrogen bond in ^{b}IC6. In the resulting intermediate ^{b}IC7, lying 33.5 kJ mol^{-1} above that of ^{b}RC, the $N5_{FAD}$ center has once again become tetrahedral (Figure 7). This causes the $N5_{FAD}$—$C1_{Gal}$ linkage to weaken and hence lengthen considerably by 0.19 Å to 1.62 Å. As a result, the $C1_{Gal}$ center is now again susceptible to substitution. In particular, it is noted that the UDP phosphate oxygen (UDP−O^{-}) initially cleaved from $C1_{Gal}$ in the first step of the overall mechanism is situated 3.89 Å from $C1_{Gal}$ in ^{b}IC7, hydrogen bonded to the guanidinium of Arg174.

Indeed, the final step in the overall mechanism is nucleophilic attack by a phosphate oxygen of the UDP moiety at the furanose's $C1_{Gal}$ center to form the final UDP-Gal*f* product complex (^{b}PC). This occurs via ^{b}TS8 with a barrier of 44.2 kJ mol^{-1} with respect to ^{b}IC7, or 77.7 kJ mol^{-1} relative to ^{b}RC (Figure 3). In ^{b}PC, lying only 11.8 kJ mol^{-1} above ^{b}RC, the $N5_{FAD}$···$C1_{Gal}$ distance has now increased considerably to 3.53 Å, that is, the *N*-glycosidic sugar-cofactor cross-link has been cleaved (Figure 7). Meanwhile, a UDP phosphate oxygen–$C1_{Gal}$ bond has been reformed with a length of 1.47 Å.

The reactant, product, and intermediate complexes observed along the above overall mechanism using the above DFT-cluster approach are summarized in Scheme 3. It is noted that for the corresponding DFT-cluster model in which His60 is protonated, the lowest energy pathway obtained followed the same analogous sequence (Figure S1). Similarly, the highest overall barrier again occurred for the second last step: tautomerization of the reformed FADH^{-} covalently bonded cofactor (i.e., ^{b}TS7: ^{b}IC6 → ^{b}IC7).

3.3. Catalytic Mechanism Obtained Using the QM/MM Model. In the DFT-cluster approach, the residues and protein environment surrounding the active site are simply and implicitly modeled as a homogeneous polar continuum. Thus, in order to explicitly consider the effects of these residues, their sterics and the nonhomogenous polarity of the surrounding environment on the above catalytic mechanism, an ONIOM QM/MM approach was used (see Computational Methods). The catalytic pathway obtained is shown in Figure 8 and, overall, is the same as that obtained using the DFT-cluster approach. However, several key differences in the optimized structures of the various complexes and, in particular, their relative energies were observed.

For instance, in contrast to the single Arg280···substrate interaction observed in ^{b}RC, in the QM/MM optimized reactant complex RC, Arg280 is now hydrogen bonded to both a phosphate oxygen of the substrate's UDP moiety *and* its pyranose ring oxygen (O_5). In addition, Arg174 hydrogen bonds with both phosphates of the UDP.

These additional phosphate···arginyl interactions help stabilize the negative charge on the substrate's phosphate groups. Indeed, the barrier for the first step, the S_N2 nucleophilic attack of $N5_{FAD}$ at $C1_{Gal}$ to form an $N5_{FAD}$(H)—$C1_{Gal}$ cross-link with concomitant dissociation of the UDP moiety, occurs via TS1 with a barrier now of only 79.1 kJ mol^{-1} (Figure 8); a decrease of 40.0 kJ mol^{-1} from that observed for ^{b}TS1 (cf. Figure 3). The comparatively "earlier" occurrence of TS1 in the reaction step than ^{b}TS1 is also illustrated by the fact that in the former, the $_{UDP}$O···$C1_{Gal}$ distance is 0.03 Å shorter at 2.02 Å, while the $N5_{FAD}$···$C1_{Gal}$

dx.doi.org/10.1021/jp310952c | J. Phys. Chem. B 2012, 116, 14040−14050

distance is significantly longer by 0.77 Å at 3.37 Å (Table S3). Again, a shift toward planarity of the $C1_{Gal}$ center and slight increased pyramidalization of $N5_{FAD}$ is observed (Table S3). It is also noted that during this step, four tyrosyl residues in the MM layer also hydrogen bond with the substrate's pyrophosphate group, helping to further stabilize its anionic charge. The resulting flavin-Gal*p* covalently bonded complex IC1 has an elongated N-glycosidic bond with $r(N5_{FAD}—C1_{Gal})$ = 1.61 Å. Furthermore, it lies 40.3 kJ mol^{-1} higher than RC (Figure 8), a decrease of 15.5 kJ mol^{-1} compared to the DFT-cluster results (cf. Figure 3).

The barrier for the subsequent tautomerization to give the $C4_{FAD}$−OH containing complex IC2 occurs via TS2 and is similarly reduced by approximately 37.2 kJ mol^{-1} to 74.7 kJ mol^{-1} relative to RC (Figure 8). This may reflect in part the lower relative energy of IC2 which, unlike that observed on the DFT-cluster PES (cf. Figure 3), now lies *below* that of RC by −3.3 kJ mol^{-1}. It should also be noted that no suitably positioned residues were observed in IC2 that may be able to help stabilize a build-up of negative charge on the $O5_{Gal}$ center. The nearest residue hydrogens were those of an R-group methyl of Ile61 (4.10 Å) and a $-CH_2-$ of Pro59 (3.72 Å) (see Table S3). Consequently, opening of the pyranose ring, cleavage of the $O5_{Gal}—C1_{Gal}$ bond, again occurs with concomitant transfer of the proton from the $C4_{FAD}$−OH group onto $O5_{Gal}$. This proceeds via TS3 at a cost of 47.1 kJ mol^{-1} relative to RC (Figure 8), only 5.0 kJ mol^{-1} lower than that obtained using the DFT-cluster approach. The resulting imine covalently bonded flavin-linear sugar intermediate IC3 is 30.6 kJ mol^{-1} higher in energy than RC (Figure 8). This is an increase of 16.7 kJ mol^{-1} compared to that obtained for the analogous reaction on the DFT-cluster PES (cf. Figure 3). It is noted that of the three "linear" sugar-containing intermediates encountered along the QM/MM mechanism pathway (IC3, IC4 and IC5), the IC3 conformation is the highest in energy (Figure 8). This is the opposite of that obtained using the DFT-cluster method (cf. Figure 3). As observed in the analogous complex ^{b}IC3 (cf. Figure 5), the newly formed $-O5_{Gal}H$ group is hydrogen bonded to the flavin's regenerated $C4_{FAD}$═O carbonyl oxygen with a length of 1.90 Å (Table S3). Thus, again, the substrate−cofactor complex must undergo a conformational change so as to favorably position the $-O4_{Gal}H$ oxygen for nucleophilic attack at the $C1_{Gal}$═$N5_{FAD}$ carbon center. It is also noted that this open chain sugar intermediate obtained using both the DFT-cluster and QM/MM approaches appears to support experimental evidence directly or indirectly obtained by UV−vis,[10] mass spectral analysis,[10] and 1H NMR spectrum experiments[6] for such an intermediate.

In fact, the rate-limiting step on the QM/MM PES is calculated to be the conformational change in which the $-O5_{Gal}H$ group rotates so that it instead hydrogen bonds to a phosphate oxygen of the cleaved UDP moiety rather than the flavin's C4═O carbonyl oxygen. This occurs via TS4 at a cost of 99.2 kJ mol^{-1} relative to RC. This is 59.2 kJ mol^{-1} higher than that obtained using the DFT-cluster approach (cf. Figure 1)! This markedly higher barrier is likely due at least in part to destabilization of TS4 by the electrostatics of the surrounding environment. Indeed, at the ONIOM(B3LYP/6-311+G(2df,p):AMBER)-ME level of theory (i.e., without inclusion of electrostatic effects) the barrier for TS4 is calculated to be 44.6 kJ mol^{-1}. This value is in good agreement with that obtained using the DFT-cluster approach (cf. Figure 3). It is also noted that the residues in the vicinity of the $-O5_{Gal}H$ group in TS4 are predominantly hydrophobic (Table S3). Thus, they do not facilitate the conformational change through, for instance, favorable polar or hydrogen bonding interactions. This calculated barrier is ∼30 kJ mol^{-1} higher than the Gibbs free energy for the rate-limiting barrier obtained by the experimental studies of Chad et al.[18] However, this is expected due to the fact that our calculated value does not include zero-point vibrational energy, enthalpy, or entropy corrections which generally give lower calculated barriers. In the resulting complex IC4, lying only slightly higher in energy than RC by 6.9 kJ mol^{-1}, the $-O5_{Gal}H$ and $-O4_{Gal}H$ groups are hydrogen bonded with a UDP phosphate oxygen and the $C4_{FAD}$═O oxygen, respectively.

Similar to that observed using the DFT-cluster approach, a further slight conformational change is required in order to reposition the $-O4_{Gal}H$ oxygen for nucleophilic attack at the $C1_{Gal}$═$N5_{FAD}$ carbon. This step occurs via TS5 with a barrier of 56.4 kJ mol^{-1} relative to RC to give the alternate conformer IC5 (Figure 8). In contrast to that observed with the above DFT-cluster approach, the latter complex is quite low in energy at 14.8 kJ mol^{-1} with respect to RC. Additionally, it is no longer calculated to be able to undergo a thermodynamically barrierless rearrangement back to IC4. Notably, the $O4_{Gal}$ oxygen is now similarly positioned to $O5_{Gal}$ in IC3: almost above and in proximity to the $C1_{Gal}$ center.

Indeed, nucleophilic attack of $O4_{Gal}$ at $C1_{Gal}$ occurs via TS6 with a low cost of only 26.2 kJ mol^{-1} relative to RC (Figure 8). In contrast to that observed on the DFT-cluster PES (cf. Figure 3), the resulting *N*-glycosidic covalently bonded flavin tautomer-furanose intermediate IC6 lies 10.9 kJ mol^{-1} *lower* in energy than RC. This is likely due, however, to enhanced stabilization of mechanistic intermediates and products in general using the extended QM/MM model. For instance, at the QM/MM level, the relative energies of all intermediates, except IC3, is lowered by 12.7−63.2 kJ mol^{-1} with respect to that observed on the DFT-cluster PES (cf. Figure 3).

Using the DFT-cluster method, the subsequent tautomerization reaction via ^{b}TS7, i.e., conversion of the $C4_{FAD}$−OH containing tautomer to that having a tetrahedral protonated $N5_{FAD}$ center, had the overall highest barrier at 120.0 kJ mol^{-1} (Figure 3). At the QM/MM level, however, this barrier is reduced by 44.4 kJ mol^{-1} to 75.6 kJ mol^{-1} (TS7) relative to RC and is no longer the rate-limiting step. The tautomeric intermediate IC7 lies markedly lower in energy than RC by 29.7 kJ mol^{-1}. Furthermore, it contains a tetrahedral $N5_{FAD}$ center with an $N5_{FAD}—C1_{Gal}$ glycosidic bond length of 1.56 Å, which is 0.06 Å shorter than observed in ^{b}IC7, i.e., at the DFT-cluster level (cf. Figure 7). However, it is markedly lower in energy than the corresponding pyranose-cofactor complex IC1 by 70.0 kJ mol^{-1}. At the DFT-cluster level, ^{b}IC7 was only modestly lower in energy than ^{b}IC1 by 22.3 kJ mol^{-1} (cf. Figure 3). This noticeably lower relative energy for IC7 may in part reflect a reduction in intramolecular strain. For instance, in the optimized structures of ^{b}IC7 and IC1, there is an intramolecular hydrogen bond between $O4_{FAD}$ and the sugar's $-O3_{Gal}H$ or $-O4_{Gal}H$ groups, respectively. By contrast, in the optimized structure of IC7, the $C4_{FAD}O$ and $-O3_{Gal}H$ groups instead form intermolecular hydrogen bonds with the backbone amide of Leu252 and the R-group of Asp351 via a water molecule, respectively. This helps to reduce the strain in the sugar-cofactor complex as illustrated by the fact that the $N5_{FAD}—C1_{Gal}$ bond length in IC7 (1.70 Å) is 0.09 and 0.08 Å longer than observed in IC1 or ^{b}IC7, respectively.

The final step is again nucleophilic attack of an oxygen of the terminal phosphate of the UDP moiety at the furanose's $C1_{Gal}$ center with concomitant cleavage of the $N5_{FAD}$—$C1_{Gal}$ bond. For this reaction, the barrier via TS8 is only 33.2 kJ mol^{-1} higher than IC7 or 3.5 kJ mol^{-1} with respect to RC. This is 69.6 kJ mol^{-1} lower than that obtained using the DFT-cluster model (Figure 3). The "earlier" occurrence of TS8 compared to ^{b}TS8 in the reaction is illustrated by the fact the forming $_{UDP}O\cdots C1_{Gal}$ bond is 0.29 Å longer at 2.38 Å while the cleaving $C1_{Gal}\cdots N5_{FAD}$ bond is 0.03 Å shorter at 2.52 Å (Table S3). Furthermore, the cleaved flavin moiety formally regenerates the FADH$^-$ cofactor. The resulting final active site bound-product complex PC is significantly lower in energy than RC by −74.2 kJ mol^{-1} (Figure 8). Hence, unlike the overall endergonic mechanism obtained using the DFT-cluster approach (Figure 3), using the QM/MM approach it is now thermodynamically favored, being notably exergonic. This may be partly due to the fact that, unlike for RC, all of the sugar hydroxyl groups and the nonbridging phosphate oxygen's in PC form hydrogen bonds with active site residues, in particular the four Tyr residues (314, 349, 185, 198), Asp351, His63 and Asn84.

It is noted that, experimentally, the effectiveness of several possible antimycobacterial agents as potential inhibitors of UGM has been examined, including sugar substrate analogues and some small compounds.[5,7,14,15,19] The above DFT-cluster and QM/MM results clearly indicate the importance of tautomerization involving $N5_{FAD}$−H, $O4_{FAD}$, $O4_{Gal}$ and $-O5_{Gal}$H. Indeed, *in silico* substitution of $O4_{FAD}$ by S within the present QM/MM model increased the relative energy of TS2 (i.e., H$^+$ transfer from $N5_{FAD}$−H to $S4_{FAD}$) to 167.7 kJ mol^{-1}. Similar substitutions of, for instance, $-O5_{Gal}$H by a thiol or amine could provide important experimental insights into the mechanism outlined herein as well as provide a basis for further enzyme kinetic and inhibition studies on UGM.

4. CONCLUSIONS

The complementary use of DFT-cluster and ONIOM QM/MM approaches have been used to obtain new insights into possible reactions involved in the catalytic mechanism of the flavoenzyme UGM and their feasibility. This has included not only examination of possible reactions involving the substrate UDP-Gal*p* and the fully reduced flavin cofactor (FADH$^-$), but also the potential role(s) of various active site residues and the protein environment in general.

The first step in the overall mechanism is nucleophilic attack of the flavin's $N5_{FAD}$ center at the anomeric carbon $C1_{Gal}$ of the substrate's sugar moiety with concomitant heterolytic cleavage of the substrate's UDP phosphate oxygen−$C1_{Gal}$ bond. Consistent with the S_N2 reaction process proposed by Soltero-Higgin et al. (Scheme 2), this results in the formation of a tetrahedral-$N5_{FAD}$ intermediate (^{b}IC1/IC1). This is then followed by a series of tautomerization reactions involving transfer of the $N5_{FAD}$−H proton that lead to and result in opening of the Gal*p* ring. Specifically, the flavin moiety first undergoes a tautomerization with the proton being transferred from $N5_{FAD}$ onto the $C4_{FAD}$=O oxygen to give a $C4_{FAD}$−OH containing complex (^{b}IC2/IC2). The proton is then transferred onto the ring oxygen $O5_{Gal}$ resulting in the formation of a linear galactose sugar (^{b}IC3/IC3); a chain-ring tautomerization process. This neutralization of the charge build-up on $O5_{Gal}$ during $O5_{Gal}$—$C1_{Gal}$ bond cleavage appears to be required as there are no suitable residues positioned to help stabilize an oxyanionic $O5_{Gal}$. Furthermore, it also enables the later nucleophilic attack of the $-O4_{Gal}$H oxygen at $C1_{Gal}$ to form the furanose ring, to be competitive with reattack of $O5_{Gal}$ at $C1_{Gal}$. Suitable positioning of $O4_{Gal}$ for such a nucleophilic attack is achieved via a two-step conformational rearrangement, ^{b}IC3/IC3 → ^{b}IC4/IC4 → ^{b}IC5/IC5, that results in positioning of the $-O4_{Gal}$H group over the $C1_{Gal}$ center. Furthermore, it forms a hydrogen bond to the $C4_{FAD}$=O oxygen. Furanose ring and final product formation is then achieved via the analogous reverse of the ring-opening process. Specifically, ^{b}IC5/IC5 undergoes chain-ring tautomerization to form the furanose ring-containing complex ^{b}IC6/IC6. The latter complex now also contains a $C4_{FAD}$−OH group and can then tautomerize to give the tetrahedral-$N5_{FAD}$ intermediate ^{b}IC7/IC7. Formation of the final desired product UDP-Gal*f* is achieved via nucleophilic attack of a phosphate oxygen of the UDP moiety at $C1_{Gal}$ with concomitant cleavage of the $C1_{Gal}$—$N5_{FAD}$ glycosidic bond.

In the DFT-cluster approach used herein, the highest barrier in the overall mechanism at 120.0 kJ mol^{-1} (^{b}TS7) is calculated to be tautomerization of the imine covalently bonded furanose ring-containing intermediate, in other words, transfer of the proton from $C4_{FAD}$−OH once the furanose ring has been formed (^{b}IC6) onto $N5_{FAD}$ to give the tetrahedral-$N5_{FAD}$ intermediate ^{b}IC7. This barrier is only slightly higher by 0.9 kJ mol^{-1} than that calculated for the initial nucleophilic attack of the flavin's $N5_{FAD}$ at the substrates $C1_{Gal}$ center, i.e., RC → ^{b}IC1.

More extensive inclusion of the residues and protein surrounding the active site and its nonhomogeneous polarity were modeled using a QM/MM approach. In contrast to that observed on the DFT-cluster PES, the highest overall barrier was obtained for the required conformational changes in the imine covalently bonded galactose chain-flavin intermediate. More specifically, the barrier for rotation of the $-O5_{Gal}$H group from hydrogen bonding to the $C4_{FAD}$=O oxygen to a phosphate oxygen of the initial substrate-derived UDP moiety was calculated to be 99.2 kJ mol^{-1} (TS4). Furthermore, unlike that obtained at the DFT-cluster level, the overall reaction was calculated to be quite exergonic with the final product complex (PC) lying markedly lower in energy than the initial reactant complex (RC) by 74.2 kJ mol^{-1}.

These results provide new insights into the catalytic mechanism of a novel flavoenzyme but also into the remarkable possible chemistry of flavin cofactor. In addition, they also provide insights into why an oxidized flavin cofactor appears to be a catalytic inhibitor to UGM. Specifically, the cofactor must contain an $N5_{FAD}$−H proton, which is not found in the oxidized flavin structure, so that the resulting covalent intermediate complexes can undergo tautomerization that lead to pyranose ring-opening and to furanose ring-formation. These mechanistic insights can also be used to help develop potential new inhibitors that exploit the tautomerization chemistry in the UGM mechanism.

■ ASSOCIATED CONTENT

Supporting Information

Cartesian coordinates of all optimized structures, DFT-cluster obtained PES for His60 protonated, schematic illustration of numbering used in the flavin model, table comparing key active site-substrate interactions from the X-ray crystal structures

3INT and 3HDQ. This material is available free of charge via the Internet at http://pubs.acs.org.

AUTHOR INFORMATION

Corresponding Author

*E-mail: gauld@uwindsor.ca.

Notes

The authors declare no competing financial interest.

ACKNOWLEDGMENTS

We thank the Natural Sciences and Engineering Research Council of Canada (NSERC) for funding and SHARCNET for a Graduate Student Fellowship (W.-J.H.) and additional computational resources, and Jorge Llano, Rami Gherib, and Eric A. C. Bushnell for helpful discussions.

REFERENCES

(1) World Health Organization *Global Tuberculosis Control: WHO Report 2011*, 2011.
(2) Marria, E. *Nature* **2006**, *443*, 131.
(3) Tripathi, R. P.; Tewari, N.; Dwivedi, N.; Tiwari, V. K. *Med. Res. Rev.* **2005**, *25*, 93−131.
(4) Crick, D. C.; Brennan, P. J. Biosynthesis of the arabinogalactan-peptidoglycan complex of Mycobacterium tuberculosis. In *The Mycobacteria Cell Wall*; Daffe, M., Reyrat, J.-M., Eds.; ASM Press: Washington, DC, 2008.
(5) Borrelli, S.; Zandberg, W. F.; Mohan, S.; Ko, M.; Martinez-Gutierrez, F.; Partha, S. K.; Sanders, D. A. R.; Av-Gay, Y.; Pinto, B. M. *Int. J. Antimicrob. Agents* **2010**, *36*, 364−368.
(6) Gruber, T. D.; Westler, W. M.; Kiessling, L. L.; Forest, K. T. *Biochemistry* **2009**, *48*, 9171−9173.
(7) Dykhuizen, E. C.; May, J. F.; Tongpenyai, A.; Kiessling, L. L. *J. Am. Chem. Soc.* **2008**, *130*, 6706−6707.
(8) Nassau, P. M.; Martin, S. L.; Brown, R. E.; Weston, A.; Monsey, D.; McNeil, M. R.; Duncan, K. *J. Bacteriol.* **1996**, *178*, 1047−1052.
(9) Sanders, D. A. R.; Staines, A. G.; McMahon, S. A.; McNeil, M. R.; Whitfield, C.; Naismith, J. H. *Nat. Struct. Biol.* **2001**, *8*, 858−863.
(10) Soltero-Higgin, M.; Carlson, E. E.; Gruber, T. D.; Kiessling, L. L. *Nat. Struct. Mol. Biol.* **2004**, *11*, 539−543.
(11) Koplin, R.; Brisson, J.-R.; Whitfield, C. *J. Biol. Chem.* **1997**, *272*, 4121−4128.
(12) Beverley, S. M.; Owens, K. L.; Showalter, M.; Griffith, C. L.; Doering, T. L.; Jones, V. C.; McNeil, M. R. *Eukaryotic Cell* **2005**, *4*, 1147−1154.
(13) Pedersen, L. L.; Turco, S. J. *Cell. Mol. Life Sci.* **2003**, *60*, 259−266.
(14) Partha, S. K.; Sadeghi-Khomami, A.; Slowski, K.; Kotake, T.; Thomas, N. R.; Jakeman, D. L.; Sanders, D. A. R. *J. Mol. Biol.* **2010**, *403*, 578−590.
(15) Soltero-Higgin, M.; Carlson, E. E.; Phillips, J. H.; Kiessling, L. L. *J. Am. Chem. Soc.* **2004**, *126*, 10532−10533.
(16) Gruber, T. D.; Borrok, M. J.; Westler, W. M.; Forest, K. T.; Kiessling, L. L. *J. Mol. Biol.* **2009**, *391*, 327−340.
(17) Yuan, Y.; Bleile, D. W.; Wen, X.; Sanders, D. A. R.; Itoh, K.; Liu, H.; Pinto, B. M. *J. Am. Chem. Soc.* **2008**, *130*, 3157−3168.
(18) Chad, J. M.; Sarathy, K. P.; Gruber, T. D.; Addala, E.; Kiessling, L. L.; Sanders, D. A. R. *Biochemistry* **2007**, *46*, 6723−6732.
(19) Eppe, G.; Peltier, P.; Daniellou, R.; Nugier-Chauvin, C.; Ferrières, V.; Vincent, S. P. *Bioorg. Med. Chem. Lett.* **2009**, *19*, 814−816.
(20) Barlow, J. N.; Blanchard, J. S. *Carbohydr. Res.* **2000**, *328*, 473−480.
(21) Zhang, Q.; Liu, H.-W. *J. Am. Chem. Soc.* **2001**, *123*, 6756−6766.
(22) Dhatwalia, R.; Singh, H.; Oppenheimer, M.; Karr, D. B.; Nix, J. C.; Sobrado, P.; Tanner, J. J. *J. Biol. Chem.* **2012**, *287*, 9041−9051.
(23) van Straaten, K. E.; Routier, F. H.; Sanders, D. A. R. *J. Biol. Chem.* **2012**, *287*, 10780−10790.
(24) Barlow, J. N.; Girvin, M. E.; Blanchard, J. S. *J. Am. Chem. Soc.* **1999**, *121*, 6968−6969.
(25) Partha, S. K.; van Straaten, K. E.; Sanders, D. A. R. *J. Mol. Biol.* **2009**, *394*, 864−877.
(26) Beis, K.; Srikannathasan, V.; Liu, H.; Fullerton, S. W. B.; Bamford, V. A.; Sanders, D. A. R.; Whitfield, C.; McNeil, M. R.; Naismith, J. H. *J. Mol. Biol.* **2005**, *348*, 971−982.
(27) Müller, F. *Chemistry and Biochemistry of Flavoenzymes*; CRC Press: Boca Raton, FL, 1991; Vol. *I*.
(28) Massey, V. *Biochem. Soc. Trans.* **2000**, *28*, 283−296.
(29) Joosten, V.; van Berkel, W. J. H. *Curr. Opin. Chem. Biol.* **2007**, *11*, 195−202.
(30) Zhang, Q.; Liu, H.-w. *J. Am. Chem, Soc.* **2000**, *122*, 9065−9070.
(31) Huang, Z.; Zhang, Q.; Liu, H.-w. *Bioorg. Chem.* **2003**, *31*, 494−502.
(32) Fullerton, S. W. B.; Daff, S.; Sanders, D. A. R.; Ingledew, W. J.; Whitfield, C.; Chapman, S. K.; Naismith, J. H. *Biochemistry* **2003**, *42*, 2104−2109.
(33) Yuan, Y.; Wen, X.; Sanders, D. A. R.; Pinto, B. M. *Biochemistry* **2005**, *44*, 14080−14089.
(34) Frisch, M. J.; Trucks, G. W.; Schlegel, H. B.; Scuseria, G. E.; Robb, M. A.; Cheeseman, J. R.; Scalmani, G.; Barone, V.; Mennucci, B.; Petersson, G. A. et al. *Gaussian 09*; Gaussian Inc.: Wallingford CT, 2009. (For full citation see Supporting Information, Table S4).
(35) Becke, A. D. *J. Chem. Phys.* **1993**, *98*, 1372−1377.
(36) Becke, A. D. *J. Chem. Phys.* **1993**, *98*, 5648−5652.
(37) Lee, C.; Yang, W.; Parr, R. G. *Phys. Rev. B* **1988**, *37*, 785−789.
(38) Siegbahn, P. E. M.; Blomberg, M. R. A. *Chem. Rev.* **2000**, *100*, 421−438.
(39) Noodleman, L.; Lovell, T.; Han, W. G.; Li, J.; Himo, F. *Chem. Rev.* **2004**, *104*, 459−508.
(40) Voet, D.; Voet, G. J. *Biochemistry*; 4th ed.; John Wiley & Sons, Inc.: New York, 2011.
(41) Liu, H.; Llano, J.; Gauld, J. W. *J. Phys. Chem. B* **2009**, *113*, 4887−4898.
(42) Robinet, J. J.; Cho, K. B.; Gauld, J. W. *J. Am. Chem. Soc.* **2008**, *130*, 3328−3334.
(43) Chen, S.-L.; Fang, W.-H.; Himo, F. *Theor. Chem. Acc.* **2008**, *120*, 515−522.
(44) Lundberg, M.; Siegbahn, P. E. M. *J. Chem. Phys.* **2005**, *122*, 224103−224109.
(45) Llano, J.; Gauld, J. W. Mechanistics of Enzyme Catalysis: From Small to Large Active-Site Models. In *Quantum Biochemistry*; Matta, C. F., Ed.; Wiley-VCH Verlag GmbH & Co. KGaA: Weinheim, Germany, 2010; Vol. *2*.
(46) Clemente, F. R.; Vreven, T.; Frisch, M. J. Getting the Most out of ONIOM: Guidelines and Pitfalls. In *Quantum Biochemistry*; Matta, C. F., Ed.; Wiley-VCH Verlag GmbH & Co. KGaA: Weinheim, Germany, 2010; Vol. *1*.
(47) Cornell, W. D.; Cieplak, P.; Bayly, C. I.; Gould, I. R.; Merz, K. M.; Ferguson, D. M.; Spellmeyer, D. C.; Fox, T.; Caldwell, J. W.; Kollman, P. A. *J. Am. Chem. Soc.* **1995**, *117*, 5179−5197.
(48) All acidity results were calculated by B3LYP/6-31G(d) level of theory in IEF-PCM model with ε = 4.0.
(49) Lewis, B. E.; Choytun, N.; Schramm, V. L.; Bennet, A. J. *J. Am. Chem. Soc.* **2006**, *128*, 5049−5058.
(50) Mohr, M.; Bryce, R. A.; Hillier, I. H. *J. Phys. Chem. A* **2001**, *105*, 8216−8222.
(51) Himo, F. *Theor. Chem. Acc.* **2006**, *116*, 232−240.
(52) The bond length was calculated at the B3LYP/6-31G(d) level of theory in gas phase.